J. Fluid Mech. (2022), *vol*. 937, R1, doi:10.1017/jfm.2022.107

Universality of stretching separation

David Baumgartner[1], **Günter Brenn**[1] **and Carole Planchette**[1],†

[1]Institute of Fluid Mechanics and Heat Transfer, Graz University of Technology, A-8010 Graz, Austria

(Received 20 December 2021; revised 26 January 2022; accepted 29 January 2022)

We develop a model to predict the fragmentation limit of drops colliding off-centre. The prediction is excellent over a wide range of liquid properties and it can be used without adjusting any parameter. The so-called stretching separation is attributed to the extension of the merged drop above a critical aspect ratio of 3.25. The evolution of this aspect ratio is influenced by the liquid viscosity and can be interpreted via an energy balance. This approach is then adapted to drop–jet collisions, which we model as consecutive drop–drop collisions. The fragmentation criterion is similar to that observed for drop–drop collisions, while the evolution of the stretched jet aspect ratio is modified to account for the different flow fields and geometry.

Key words: capillary flows, breakup/coalescence, jets

1. Introduction

Collisions of two or more droplets of one single liquid in a gaseous environment is a common phenomenon whose importance motivated many theoretical (Roisman 2009; Roisman, Berberović & Tropea 2009), numerical (Sun *et al.* 2015; Li 2016; Moqaddam, Chikatamarla & Karlin 2016; Huang, Pan & Josserand 2019) and experimental (Brenn, Valkovska & Danov 2001; Brenn & Kolobaric 2006; Pan, Chou & Tseng 2009) studies. Collisions may cause droplets to permanently coalesce and trigger rainfall (Jayaratne & Mason 1964). They may also lead to fragmentation and therefore to the formation of drops with different sizes and trajectories. These phenomena also occur in industrial processes, which produce or employ drops, such as coating, injection, cooling,... (Brenn, Durst & Tropea 1996). The consequences depend on the application, but can be severe. It may alter the delivery of active ingredients from spray-dried particles or modify the intake of pesticide sprayed onto crops. Thus, if not controlled, the collision outcomes must at least be predicted. Results across multiple studies reveal that coalescence, bouncing,

† Email address for correspondence: carole.planchette@tugraz.at

reflexive and stretching separations are the four main outcomes of drop–drop (D–D) collisions. Which outcome is obtained depends on the collision parameters and on the liquid drop behaviour characterized by the drop Ohnesorge number $Oh_d = \mu_d/\sqrt{\rho_d \sigma_d D_d}$, which compares the relative importance of the capillary to the viscous contribution. Here, μ_d, ρ_d, σ_d and D_d are the drop liquid viscosity, density, surface tension and the drop diameter, respectively. Note that Oh_d is independent from U, the relative drop velocity. Classically, regime maps are represented for a fixed Oh_d using the dimensionless impact parameter X, which quantifies the collision eccentricity, and the drop Weber number $We_d = \rho_d D_d U^2/\sigma_d$, which represents the ratio of inertia over capillarity (Ashgriz & Poo 1990; Jiang, Umemura & Law 1992; Qian & Law 1997; Saroka & Ashgriz 2015).

This work focuses on off-centre drop collisions, more precisely on the stretching separation causing the fragmentation of the otherwise permanently merged drop. Despite case-to-case parameters adjustment, the existing models have limited validity ranges (Gotaas *et al.* 2007; Rabe, Malet & Feuillebois 2010; Finotello *et al.* 2017; Pan *et al.* 2019). More recently, Al-Dirawi *et al.* (2021) proposed a new model free of adjustable parameters, but its derivation is empirical and its applicability limited to $0.02 < Oh_d < 0.14$. We propose a physical analysis and establish a unique, general and robust model predicting the stretching separation for D–D collisions. It is valid at least for $0.008 < Oh_d < 0.325$, i.e. over the entire experimentally screened domain. We additionally extend the concept of stretching separation to drops colliding with a continuous jet. These collisions, also called in-air microfluidics, create well-defined liquid structures (Planchette, Hinterbichler & Brenn 2017*a*), which can be solidified into fibres or capsules with high precision and throughput (Visser *et al.* 2018). Yet, studies on drop–jet (D–J) collisions remain rather rare. Chen, Chiu & Lin (2006) investigated the out-of-plane collisions of water drops with a water jet, followed by Planchette *et al.* (2017*a*, 2018), who worked with immiscible liquid pairs on in-plane collisions. In this case, the outcomes were classified according to the fragmentation of either the drops, the jet, both phases or none. While the drop fragmentation limit has been recently well studied (Baumgartner *et al.* 2020*a*; Baumgartner, Brenn & Planchette 2020*b*), that of the jet remains poorly explained. We show that the fragmentation of the jet is caused by its excessive stretching and can be predicted by considering the D–J collisions as a succession of off-centre D–D collisions. The article is organized as follows. In the next section, the experimental set-up and problem parameters are presented. Section 3 focuses first on the D–D collisions and then on the D–J collisions. The article ends with the conclusions.

2. Experimental set-up and problem parameters

All D–D and D–J collisions are carried out with the same set-up depicted in figure 1(*a*). Here and thereafter, subscript d corresponds to drop liquid properties and parameters while j refers to those of the jet. For D–D collisions, two droplet generators (Brenn *et al.* 1996) are excited with the same frequency f_d ($5\,\text{kHz} < f_d < 24\,\text{kHz}$), while for D–J collisions, only one (DG1) is activated. An LED stroboscope (illumination) is synchronized with f_d so that each picture consists of hundreds of superimposed collisions illuminated by short flashes of approximately 100 ns each. The liquids are supplied with two independent pressurized tanks. Two cameras record the collisions in front view (Cam1, observation of the drop and jet deformation, resolution up to 4 µm per pixel) and orthogonal view (Cam2, in-plane alignment of the trajectories with microtraverses).

Figure 1(*b*,*c*) shows the problem parameters associated with D–D and D–J collisions, respectively. All geometrical parameters are extracted from recorded pictures with the public-domain software ImageJ. Here D_d and D_j stand for the drop and jet

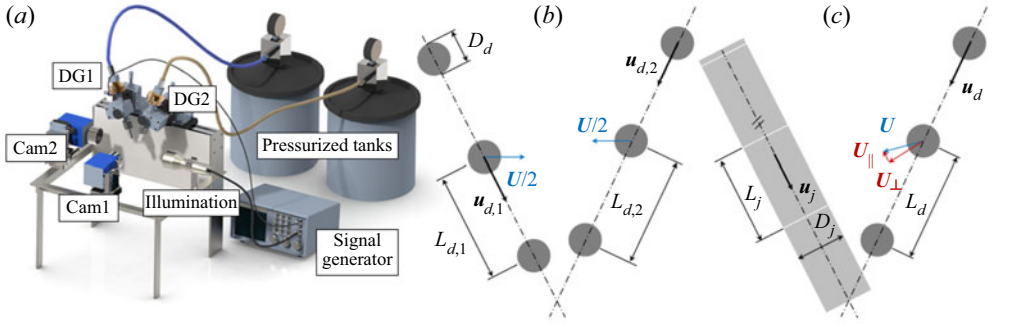

Figure 1. (*a*) Experimental set-up and problem parameters for (*b*) D–D and (*c*) D–J collisions.

diameter, respectively. For D–D collisions, $L_{d,1}$ and $L_{d,2}$ correspond to the distance between two consecutive drops of each stream. The droplet velocities are given by $\boldsymbol{u}_{d,i} = \boldsymbol{L}_{d,i} f_d$. They vary between $3\,\mathrm{m\,s^{-1}}$ and $13\,\mathrm{m\,s^{-1}}$ and provide the relative impact velocity $\boldsymbol{U} = \boldsymbol{u}_{d,2} - \boldsymbol{u}_{d,1}$, which ranges from $1.9\,\mathrm{m\,s^{-1}}$ to $5.4\,\mathrm{m\,s^{-1}}$. Practically, we use three liquids: water (W, $\rho = 995\,\mathrm{kg\,m^{-3}}$, $\mu = 0.98\,\mathrm{mPa\,s}$, $\sigma = 72.5\,\mathrm{mN\,m^{-1}}$), an aqueous glycerol solution (G, $\rho = 1125\,\mathrm{kg\,m^{-3}}$, $\mu = 5.1\,\mathrm{mPa\,s}$, $\sigma = 68.0\,\mathrm{mN\,m^{-1}}$) and one silicone oil (SO, $\rho = 949\,\mathrm{kg\,m^{-3}}$, $\mu = 18.5\,\mathrm{mPa\,s}$, $\sigma = 20.5\,\mathrm{mN\,m^{-1}}$) and vary the drop diameter between $175\,\mu\mathrm{m}$ and $367\,\mu\mathrm{m}$, covering $0.008 < Oh_d < 0.325$ with $15 < We_d < 265$.

For D–J collisions, we further introduce the spatial period of the jet $L_j = |u_j|/f_d$, where u_j is the flow-rate equivalent jet velocity ($3.5\,\mathrm{m\,s^{-1}} < |u_j| < 11.5\,\mathrm{m\,s^{-1}}$). It is deduced from the measured mass flow rate knowing the liquid density and jet section. The relative impact velocity $\boldsymbol{U} = \boldsymbol{u}_d - \boldsymbol{u}_j$ varies between $3\,\mathrm{m\,s^{-1}}$ and $8\,\mathrm{m\,s^{-1}}$ and is adjusted to be perpendicular to the jet axis. More precisely, its component parallel to the jet axis obeys $U_\parallel < 0.1U$. There, the drops are always made of the aqueous glycerol solution, while the jet consists of silicone oils. Their density and surface tension are almost constant ($845 < \rho < 949\,\mathrm{kg\,m^{-3}}$, $17 < \sigma < 20.5\,\mathrm{mN\,m^{-1}}$) while their viscosity varies between $1.4\,\mathrm{mPa\,s}$ and $18.5\,\mathrm{mPa\,s}$. With an interfacial tension of $32 \pm 3\,\mathrm{mN\,m^{-1}}$, the jet always totally wets the drops. The jet diameter is equal to $280 \pm 10\,\mu\mathrm{m}$, resulting in jet Ohnesorge numbers $0.02 < Oh_j = \mu_j/\sqrt{\rho_j D_j \sigma_j} < 0.25$. The droplet diameter varies between $190\,\mu\mathrm{m}$ and $370\,\mu\mathrm{m}$, leading to diameter ratios $0.7 < \Delta = D_d/D_j < 1.3$. Further information can also be found in Baumgartner *et al.* (2020*a*,*b*).

3. Discussion

While different in nature, D–D and D–J collisions clearly show similarities, encouraging the build of some analogy between the two collision processes, see figure 2(*a–d*). Before doing so, let us focus on D–D collisions. Our model is based on two ingredients: (i) a fragmentation criterion, which corresponds to a critical value of $\Psi_d = \max[H_d(t)/D_d]$, the maximum dimensionless drop extension (see figure 2*a*,*b*) and (ii) a function, which describes the variations of Ψ_d with the liquid properties and collision parameters.

First, $H_d(t)/D_d$ is measured for several instants after the collision and fitted with a third-order polynomial to obtain Ψ_d, its maximum value with a typical measurement uncertainty of less than 3 %, see figure 2(*e*). Note that the deformation undergone by drops colliding off-centre is not an axisymmetric lamella, as seen for head-on collisions. Thus, H_d, the maximal extension is the end-to-end length of a stretched entity and not a maximal

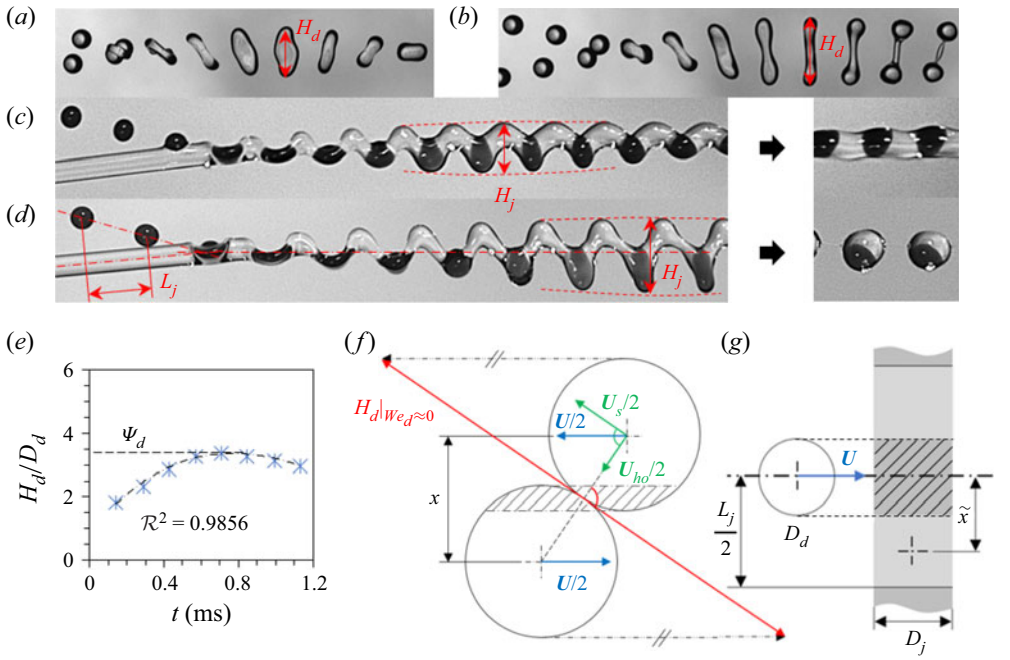

Figure 2. (*a–d*) Drop and jet trajectories go from left to right. The D–D collision in (*a*) coalescence ($D_d = 341\,\mu$m, $X = 0.41$, $We_d = 31.5$, $Oh_d = 0.033$) and (*b*) stretching separation ($D_d = 340\,\mu$m, $X = 0.61$, $We_d = 31.3$, $Oh_d = 0.033$). The D–J collision in (*c*) drops-in-jet ($D_d = 275\,\mu$m, $\tilde{X} = 1.64$, $We_d = 30$, $Oh_j = 0.246$) and (*d*) capsules ($D_d = 292\,\mu$m, $\tilde{X} = 1.86$, $We_d = 48$, $Oh_j = 0.246$). (*e*) Measured temporal evolution of H_d/D_d (symbols) and its fit (dashed line) providing its maximum, Ψ_d. Collision eccentricity for (*f*) D–D collisions, $X = x/D_d$, and (*g*) D–J collisions, $\tilde{X} = 2\tilde{x}/D_j$.

diameter. We verify that the separation threshold corresponds to a constant critical value of Ψ_d of 3.25 (dashed line in figure 3*a*), in agreement with the numerical results of Saroka & Ashgriz (2015) and the recent experimental findings of Al-Dirawi *et al.* (2021). This provides the fragmentation criterion (i). Note that this value remarkably close to π, the theoretical one (Rayleigh 1892), is obtained by normalizing the critical extension with the initial drop diameter, as done by Saroka & Ashgriz (2015); Al-Dirawi *et al.* (2021). Assuming a cylindrical shape and using volume conservation leads to a critical value of more than 5, well above the classical result of Plateau–Rayleigh.

We then derive the evolution of Ψ_d with the liquid properties and collision parameters, i.e the second ingredient of our approach. We consider a purely geometric contribution $\Psi_d|_{We_d\approx 0}$ and an inertial one $\Psi_d|_{We_d\neq 0}$. The relative velocity U is projected parallel ($\boldsymbol{U}_{ho}$) and normally ($\boldsymbol{U}_s$) to the line connecting the two drop centres at contact (see figure 2*f*). It shows how the merged drop is elongated along $\boldsymbol{U}_s$ in the absence of inertia. This elongation contributes to Ψ_d in the form of a purely geometric term $\Psi_d|_{We_d\approx 0} = H_d|_{We_d\approx 0}/D_d$, the normalized length of the red segment in figure 2(*f*). The latter is a function of the dimensionless impact parameter, $X = x/D_d$, with x, the projection normal to $\boldsymbol{U}$ of the drop-centre-to-drop-centre segment at contact. Geometric considerations give $\Psi_d|_{We_d\approx 0} = (X+1)/\sqrt{1-X^2}$, which can be linearized for $0.3 < X < 0.8$ into $\Psi_d|_{We_d\approx 0} \approx 2.7X + 0.5$. The inertial contribution is obtained by considering that some of the initial kinetic energy ($\pi\rho_d {D_d}^3 U^2/24$) is converted into surface energy of the stretched drop ($\approx \sigma_d \pi H_d D_d$) providing at first order $\Psi_d|_{We_d\neq 0} \approx f(X, Oh_d)We_d/24$ with

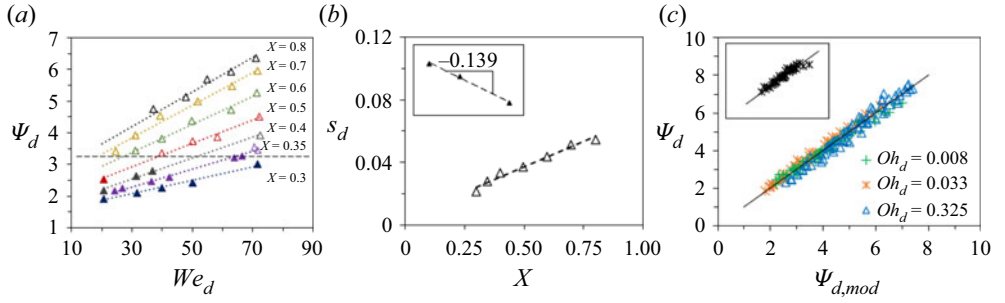

Figure 3. D–D collisions: (*a*) Ψ_d as a function of We_d for $Oh_d = 0.033$ and different X. Coalescence (full symbols) and separation (empty symbols). (*b*) $s_d = \partial\Psi_d/\partial We_d$ from (*a*). Inset: $\log(s_d/X)$ against $\log(Oh_d)$ for all experiments ($Oh_d = 0.008$, 0.033, 0.325). (*c*) Experiments vs model – (3.2). Main graph: our data ($Oh_d = 0.008$, 0.033, 0.325); inset: data of Al-Dirawi *et al.* (2021) ($0.021 \leq Oh_d \leq 0.214$, $0.24 < X < 0.55$ and $30 \leq We_d \leq 130$).

$f(X, Oh_d)$ a function that accounts for the 'relevant inertia'. Here the relevant inertia causes the merged drop to stretch. Obviously, it corresponds to the inertia of the almost unaffected drop portions that continue on their initial trajectories, see not hatched portions in figure 2(*f*). Compared with the drops' inertia, that of the almost unaffected portions must be reduced to account for their actual mass (or volume). Neglecting strong distortion, each portion volume is given by $V = (3X^2 - 2X^3)V_d$ with V_d the volume of one drop. The first inertia correction therefore corresponds to a factor $V/V_d = (3X^2 - 2X^3)$, which gives after linearization $V/V_d \approx (1.4X - 0.2)$ and thus a linear variation of $f(X, Oh_d)$ with X. This scaling ($\Psi_d|_{We_d \neq 0} \propto XWe_d$) is specific to off-centre collisions and cannot be extrapolated to head-on impacts. For $X \lesssim 0.3$, an axisymmetric lamella forms, whose maximal diameter scales as $\sqrt{We_d}$ (Wildeman *et al.* 2016; Planchette *et al.* 2017*b*). To go further, the viscous losses, i.e. the dependency with Oh_d, must be estimated.

Analytically establishing the quantitative expression of this second correction is rather complex and we decide here to use the numerical findings of Finotello *et al.* (2017). The computed normalized remaining energy is replotted as a function of X and Oh_d, see Appendix. It provides $f(X, Oh_d) \approx 0.31XOh^{-0.18}$, in agreement with the expected linear variation of f with X. Consequently, we obtain $\Psi_d|_{We_d \neq 0} \approx (0.31/24)Oh_d^{-0.18}We_d$ and thus the overall theoretical deformation:

$$\Psi_{d,th} = \alpha_{d,th}Oh_d^{m_{th}}XWe_d + \beta_{d,th}X + \gamma_{d,th}. \tag{3.1}$$

The constants $\beta_{d,th} = 2.7$ and $\gamma_{d,th} = 0.5$ come from $\Psi_d|_{We_d \approx 0}$, and $\alpha_{d,th} = 0.31/24 \approx 0.013$ and $m_{th} = -0.18$ originate from $\Psi_d|_{We_d \neq 0}$ and thus from the estimation of the relevant inertia. Due to the uncertainty of the computed findings, the approximation caused by linearization and the crude estimation of the stretched drop surface energy, we do not expect $\alpha_{d,th}$ and m_{th} to be quantitatively well predicted. We nevertheless anticipate a qualitative agreement of (3.1), which we probe by plotting the experimental data Ψ_d as a function of We_d for different X. While these curves are obtained for all experiments ($0.008 < Oh_d < 0.325$), only those corresponding to $Oh_d = 0.033$ are shown in figure 3(*a*). Note that the line corresponding to $\Psi_d = 3.25$ separates well the coalescence (full symbols) from the separation (empty symbols). In agreement with (3.1), Ψ_d increases linearly with We_d. Saroka & Ashgriz (2015), who numerically studied water drop collisions, reported similar variations. Further, for a given Oh_d and fixed X, the curve slopes s_d are linear in X (figure 3*b*) as expected by (3.1) (first term). Repeating the experiments with three liquids and thus three Oh_d, we find that $a_d = s_d/X$ is equal to

0.078 for W ($Oh_d = 0.008$), 0.066 for G ($Oh_d = 0.033$) and 0.047 for SO ($Oh_d = 0.325$), and thus decreases with increasing Oh_d. The scaling $a_d \propto {Oh_d}^{-0.14}$ (see dashed line in the insert of figure 3*b*) is reasonably well captured by (3.1), which predicts $a_d \propto {Oh_d}^{-0.18}$.

To obtain a quantitative agreement, the experimental results Ψ_d are fitted by the model equation $\Psi_{d,mod} = \alpha_{d,mod} Oh_d^{m_{mod}} XWe_d + \beta_{d,mod} X + \gamma_{d,mod}$. There, m_{mod} and $\alpha_{d,mod}$ are only adjusted once, while $\beta_{d,mod}$ and $\gamma_{d,mod}$ are taken equal to their theoretical values, $\beta_{d,th}$ and $\gamma_{d,th}$, see figure 3(*c*). We obtain an excellent prediction with

$$\Psi_{d,mod} = 0.041 Oh_d^{-0.128} XWe_d + 2.7X + 0.5. \tag{3.2}$$

The discrepancy between m_{th} and m_{mod} (28 %) could originate from the integration by Finotello *et al.* (2017) of the losses over the whole process instead of the first instants, see Appendix for details. The fit also provides $\alpha_{d,mod} = 0.041$, while the theory gives $\alpha_{d,th} = 0.013$. The difference (factor 3) can be explained by the crude estimation of the stretched drop surface. All constants being the same, at least for $0.008 < Oh_d < 0.325$, (3.2) constitutes a model which is valid over a very wide domain without the need for any adjustment. The agreement is also excellent while using the data of Al-Dirawi *et al.* (2021) (inset of figure 3*c*). This indeed indicates that the stretching separation is not purely inertial as previously reported by Al-Dirawi *et al.* (2021). In fact, the authors probed fewer values of We_d over a smaller range of Oh_d, which did not allow to identify the variations of $\partial\Psi_d/\partial X$ with Oh_d.

We then predict the separation threshold in the form of an (X, We_d) relation by fixing in (3.2) $\Psi_{d,mod}$ to its critical value of 3.25. The results are compared to those of the literature, see figure 5(*a–c*). First of all, for all considered Oh_d, the predicted thresholds (continuous lines) perfectly match the experimental ones (symbols). We further observed a very good agreement to previously proposed models, which involved adjusted parameters while being limited to given values or narrow ranges of Oh_d (Ashgriz & Poo 1990; Jiang *et al.* 1992; Gotaas *et al.* 2007; Finotello *et al.* 2017). We recall that with our approach no parameter is adjusted to cover collisions with $0.008 < Oh_d < 0.325$.

Let us now apply these results to D–J collisions. In former studies (Planchette *et al.* 2018; Baumgartner *et al.* 2020*a*,*b*), the spatial period of the jet L_j was normalized by D_j and used to build a pseudo-Rayleigh criterion. A critical value of 2 was found to roughly describe the jet fragmentation threshold in the limit of moderate jet viscosity. Here, the analogy with D–D collisions requires the introduction of a new parameter to quantify the eccentricity of the successive collisions. As sketched in figure 2(*g*), these collisions involve a drop and the jet portions found before and after this drop (lighter grey). Note that the jet portion directly impacted by the drop (hatched) is associated with the drop to form a compound drop. Thus, the distance between the centre of mass of the compound drop and that of the jet portions found before or after is given by $\tilde{x} = (L_j + D_d)/4$. This distance is counted twice since each compound drop interacts with two such jet sections. Using D_j for normalization, the equivalent impact parameter reads $\tilde{X} = (L_j + D_d)/(2D_j)$.

We record several D–J collisions and define, similarly to $H_d(t)/D_d$, the dimensionless extension of the jet $H_j(t)/D_j$, which is measured perpendicularly to the final D–J compound trajectory (figure 2*c*,*d*). Its temporal evolution is fitted by a third-order polynomial providing its maximum value $\Psi_j = \max(H_j(t)/D_j)$. The procedure and accuracy is similar to that of D–D collisions, see figure 2(*e*).

We first confirm that the jet fragmentation corresponds to a critical value of Ψ_j, see figure 4(*a*). Interestingly, this critical value is 3.0, thus remarkably close to that found for the D–D stretching separation and underlines the relevance of our analogy. We then plot for different $\tilde{X}$, the evolution of Ψ_j with We_d and evidence a linear dependency similar to

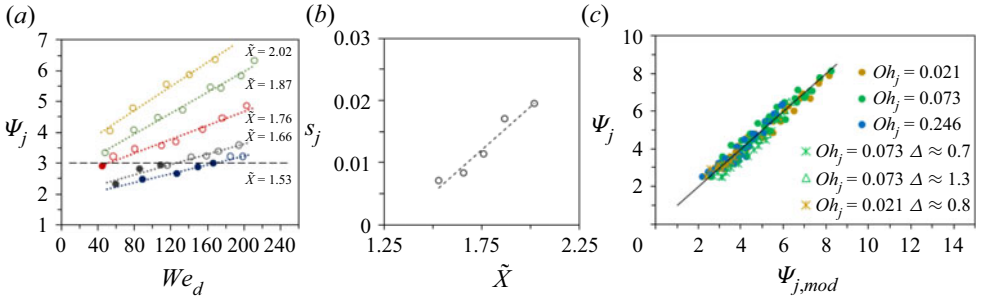

Figure 4. D–J collisions: (*a*) Ψ_j against We_d for different $\tilde{X}$, $Oh_j = 0.246$ and $\Delta = 1.0$. Coalescence (full symbols) and separation (empty symbols); (*b*) $s_j = \partial\Psi_j/\partial We_d$ against $\tilde{X}$ from (*a*); (*c*) experiments vs model (3.3) with $0.021 < Oh_j < 0.25$ and $0.7 < \Delta < 1.3$.

Ψ_d for D–D collisions. The curve slopes, s_j, are again linear in $\tilde{X}$ (figure 4*b*) and increase with Oh_j. For D–J collisions, the relevant Ohnesorge number is that of the jet liquid, since the viscous losses mainly take place in the interstitial jet portions, which are the most stretched. We therefore propose to describe the jet stretching as

$$\Psi_{j,mod} = \alpha_j Oh_j^n \tilde{X} We_d + \beta_j Oh_j^n \tilde{X} + \gamma_j. \tag{3.3}$$

Here again, α_j, β_j and γ_j are constants. The first term accounts for the drop inertia reduced by viscous losses taking place in the jet liquid only. The last two terms correspond to geometrical effects. As shown in figure 4(*c*), the agreement is again very good. The fit provides -0.10 for the exponent n, close to -0.128 found for m_{mod} and therefore supports the assumption that the viscosity (of drop and jet) plays, despite different geometries, a similar role in both processes (D–D and D–J collisions, respectively). Here α_j, β_j and γ_j are found to be +0.0066, +3.98 and -5.85, respectively. The slight deviation observed for D–J could have several origins. First of all, the system centre of mass is approximated by that of the jet, which slightly affects the measurement of the collision inertia. Second, immiscible liquids are used, which modify the flow field and thus the viscous losses. Due to the lack of existing data, (3.3) could not yet be tested against results obtained with miscible liquids. It should definitively be done in future investigations. Finally and despite its similarities, the process itself is different. For D–J collisions, the system is continuous, and mainly shear occurs between the colliding elements. For D–D, the drop pairs constitute a close system, which can rotate around their centre of mass, consuming part of the available inertia.

To explain why, in contrast to $\Psi_d|_{We_d \approx 0}$, $\Psi_j|_{We_d \to 0} = \beta_j Oh_j^n \tilde{X} + \gamma_j$ is a function of Oh_j, it is useful to recall that Ohnesorge numbers can be seen as the ratio of a bulk motion time scale, $t_\mu = \mu_j D_j/\sigma_j$ (Stone & Leal 1989), and an interfacial time scale, $t_\sigma = \sqrt{\rho_j {D_j}^3/\sigma_j}$ (Rayleigh 1892). At intermediate time scales, when Ψ_j is measured, the morphology of the compound jet depends on their relative kinetics and therefore on the jet liquid properties via its Ohnesorge number. For high Oh_j, $t_\mu > t_\sigma$, the capillary effects are fast enough to significantly flatten the outer jet surface, leading to small $\Psi_j|_{We_d \to 0}$. The contrary happens for small Oh_j. We also verify that increasing L_j or D_d as well as decreasing D_j (thus increasing $\tilde{X}$) leads – as expected – to greater $\Psi_j|_{We_d \to 0}$.

Note that given the definition of $\tilde{X}$ and the value of β_j, γ_j must be negative to represent separated successive and not overlapping drop collisions. We verify that $\Psi_j|_{We_j \to 0} > 1$ in all experiments.

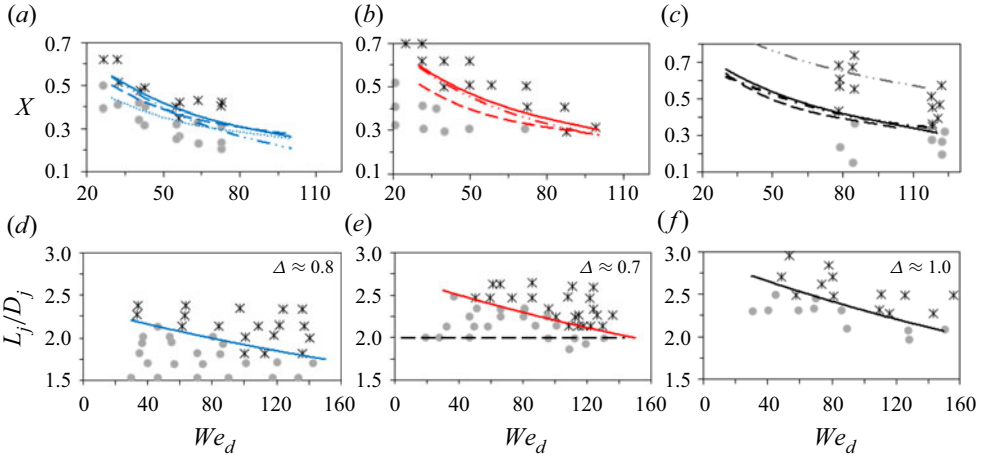

Figure 5. (*a–c*) The D–D collisions: separation transition for $Oh_d = 0.008$ (*a*), $Oh_d = 0.033$ (*b*) and $Oh_d = 0.325$ (*c*) with coalescence (circles) and separation (stars). Solid lines, (3.2) with $\Psi_{d,mod} = 3.25$; dashed lines, Jiang *et al.* (1992); dash-double-dotted lines, Finotello *et al.* (2017); dotted line, Ashgriz & Poo (1990); dot-dashed line, Gotaas *et al.* (2007). (*d–f*) The D–J collisions: transition between continuous (circles) and fragmented jet (stars) for $Oh_j = 0.021$ (*d*), $Oh_j = 0.073$ (*e*) and $Oh_j = 0.246$ (*f*). Solid lines: (3.3) with $\Psi_{j,mod} = 3.0$. Dashed line (*e*): former criterion $L_j/D_j = 2$.

As for D–D collisions, fixing $\Psi_{j,mod}$ to 3.0 in (3.3) enables the prediction of the transition between continuous (circles) and fragmented jet (diamonds), see solid lines in figure 5(*d–f*). The agreement between the model (solid lines) and the experiments (symbols) is very good, significantly better than with the former criterion of $L_j/D_j \approx 2.0$ (horizontal dashed line). It is valid over a wide range of Oh_j ($0.021 < Oh_j < 0.246$) and for different drop and jet diameters ($0.7 < \Delta < 1.3$) without adjusting any parameter.

4. Conclusions

In conclusion, we have investigated off-centred D–D and D–J collisions and found a universal model for the transition between coalescence and fragmentation caused by stretching separation. Our approach is based on (i) a simple transition criterion based on a critical drop or jet extension of 3.25 or 3.0, and (ii) the evolution of this drop or jet extension with the liquid properties and collision parameters. In contrast to other models of D–D collisions, our model remains valid for a wide range of Ohnesorge numbers – at least over $0.008 < Oh_d < 0.325$ – without adjusting any parameter. For D–J collisions, our model is valid at least for $0.02 < Oh_j < 0.25$ and $0.7 < \Delta < 1.3$ with a precision going far beyond the existing approach based on a critical L_j/D_j. The similarities between the collision morphologies, the fragmentation criterion ($\Psi_d = 3.25$ and $\Psi_j = 3.0$) and the evolution of the maximum drop or jet extension (linear in We_d, linear in X or $\tilde{X}$ and modulated by Oh to the power of m or n) underline the universality of our approach and of the so-called stretching separation. It could certainly be successfully applied to further situations, such as miscible D–J collisions and beyond.

Funding. We would like to thank the Austrian Science Fund (FWF) for the financial support under grant no. P31064-N36.

Declaration of interests. The authors report no conflict of interest.

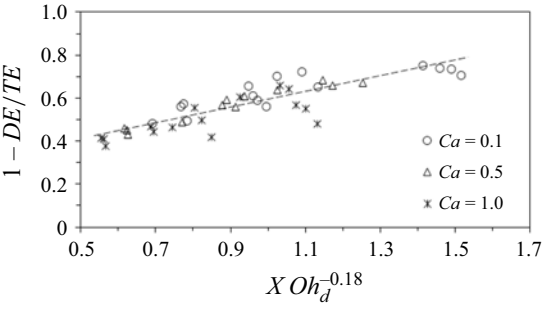

Figure 6. $(1 - DE/TE)$ – the energy, which is left for droplet stretching – as a function of X and Oh_d. The dashed line corresponds to $1 - DE/TE = 0.31XOh_d^{-0.18} + 0.25$.

Author ORCIDs.
David Baumgartner https://orcid.org/0000-0003-2505-3742;
Günter Brenn https://orcid.org/0000-0001-7576-0790;
Carole Planchette https://orcid.org/0000-0002-3974-5742.

Appendix. Viscous losses

To estimate the viscous losses taking place in the first part of D–D collisions, we make use of the numerical results of Finotello *et al.* (2017). More precisely, we replot the data of their figure 9. In its original form, it represents the variations of the dissipated energy DE over the total initial energy TE (approximated by the initial kinetic energy) as a function of the impact parameter X for different capillary numbers $Ca = \mu_d U/\sigma_d$ and Weber numbers: $X \in [0.3, 0.8]$ and $Oh_d = Ca_d/\sqrt{We_d} \in [0.01, 0.20]$. From these results, we derive the normalized remaining energy $(1 - DE/TE)$, which we plot as a function of X and a power of Oh_d (see figure 6). The linear increase with X is expected since the region of high dissipation rate grows linearly for decreasing X, see Finotello *et al.* (2017). We further choose to use Oh_d as it is commonly employed to weight the relative importance of viscosity and capillarity, the inertia being here indirectly accounted for via the normalization with the total initial energy, which is approximated by the initial kinetic energy. By doing so, the best fit reveals that the remaining energy, which is left for stretching the ligament between the drops, scales as $(1 - DE/TE) \propto XOh_d^{-0.18}$. It is worth noting that Finotello *et al*. consider the duration of the entire collision process. For low Oh_d ($Oh_d \approx 0.02$, see figure 5(a) of Finotello *et al.* 2017), up to 23 % of the calculated losses arise after Ψ_d has been reached. For larger Oh_d ($Oh_d \approx 0.1$, see figure 5(b) of Finotello *et al.* 2017), these subsequent losses are more limited, in the range of 6 %. This may lead to an overestimation of the viscous losses in the case of small Oh_d and could explain why in our model, which considers only the first phase of the collision until Ψ_d is reached, an exponent of -0.128 in (3.2) provides a better agreement than the value of -0.18.

Finally, extrapolating this scaling to head-on collisions shows that approximately 25 % of the initial energy remains. While in reasonable agreement with the 35 % found by Planchette *et al.* (2017*b*), the comparison is questionable. Off-centre and head-on collisions give rise to different deformation and flow fields, which call for separate modelling. With E_μ, the viscous losses until maximal extension, and E_k, the initial kinetic energy, we have $E_\mu \approx 0.65E_k$ for $X \approx 0$ and $E_\mu \approx (0.75 - 0.31XOh_d^{-0.18})E_k$ for $0.3 \lesssim X$. How to connect these scalings remains an open question.

References

Al-Dirawi, K.H., Al-Ghaithi, K.H.A., Sykes, T.C., Castrejón-Pita, J.R. & Bayly, A.E. 2021 Inertial stretching separation in binary droplet collisions. *J. Fluid Mech.* **927**, A9.

Ashgriz, N. & Poo, J.Y. 1990 Coalescence and separation in binary collisions of liquid drops. *J. Fluid Mech.* **221**, 183–204.

Baumgartner, D., Bernard, R., Weigand, B., Lamanna, G., Brenn, G. & Planchette, C. 2020*a* Influence of liquid miscibility and wettability on the structures produced by drop–jet collisions. *J. Fluid Mech.* **885**, A23.

Baumgartner, D., Brenn, G. & Planchette, C. 2020*b* Effects of viscosity on liquid structures produced by in-air microfluidics. *Phys. Rev. Fluids* **5**, 103602.

Brenn, G., Durst, F. & Tropea, C. 1996 Monodisperse sprays for various purposes – their production and characteristics. *Part. Part. Syst. Charact.* **13** (3), 179–185.

Brenn, G. & Kolobaric, V. 2006 Satellite droplet formation by unstable binary drop collisions. *Phys. Fluids* **18** (8), 087101.

Brenn, G., Valkovska, D. & Danov, K.D. 2001 The formation of satellite droplets by unstable binary drop collisions. *Phys. Fluids* **13** (9), 2463–2477.

Chen, R.-H., Chiu, S.-L. & Lin, T.-H. 2006 Collisions of a string of water drops on a water jet of equal diameter. *Exp. Therm. Fluid Sci.* **31** (1), 75–81.

Finotello, G., Padding, J.T., Deen, N.G., Jongsma, A., Innings, F. & Kuipers, J.A.M. 2017 Effect of viscosity on droplet-droplet collisional interaction. *Phys. Fluids* **29** (6), 067102.

Gotaas, C., Havelka, P., Jakobsen, H.A., Svendsen, H.F., Hase, M., Roth, N. & Weigand, B. 2007 Effect of viscosity on droplet-droplet collision outcome: experimental study and numerical comparison. *Phys. Fluids* **19** (10), 102106.

Huang, K.-L., Pan, K.-L. & Josserand, C. 2019 Pinching dynamics and satellite droplet formation in symmetrical droplet collisions. *Phys. Rev. Lett.* **123**, 234502.

Jayaratne, O.W. & Mason, B.J. 1964 The coalescence and bouncing of water drops at an air/water interface. *Proc. R. Soc. Lond.* A **280** (1383), 545–565.

Jiang, Y.J., Umemura, A. & Law, C.K. 1992 An experimental investigation on the collision behaviour of hydrocarbon droplets. *J. Fluid Mech.* **234**, 171–190.

Li, J. 2016 Macroscopic model for head-on binary droplet collisions in a gaseous medium. *Phys. Rev. Lett.* **117**, 214502.

Moqaddam, A.M., Chikatamarla, S.S. & Karlin, I.V. 2016 Simulation of binary droplet collisions with the entropic lattice Boltzmann method. *Phys. Fluids* **28** (2), 022106.

Pan, K.-L., Chou, P.-C. & Tseng, Y.-J. 2009 Binary droplet collision at high weber number. *Phys. Rev.* E **80**, 036301.

Pan, K.-L., Huang, K.-L., Hsieh, W.-T. & Lu, C.-R. 2019 Rotational separation after temporary coalescence in binary droplet collisions. *Phys. Rev. Fluids* **4**, 123602.

Planchette, C., Hinterbichler, H. & Brenn, G. 2017*a* Drop stream – immiscible jet collisions: Regimes and fragmentation mechanisms. In *Proceeding of the 27th European Conference on Liquid Atomization and Spray Systems* (ed. R. Payri & X. Margot).

Planchette, C., Hinterbichler, H., Liu, M., Bothe, D. & Brenn, G. 2017*b* Colliding drops as coalescing and fragmenting liquid springs. *J. Fluid Mech.* **814**, 277–300.

Planchette, C., Petit, S., Hinterbichler, H. & Brenn, G. 2018 Collisions of drops with an immiscible liquid jet. *Phys. Rev. Fluids* **3**, 093603.

Qian, J. & Law, C.K. 1997 Regimes of coalescence and separation in droplet collision. *J. Fluid Mech.* **331**, 59–80.

Rabe, C., Malet, J. & Feuillebois, F. 2010 Experimental investigation of water droplet binary collisions and description of outcomes with a symmetric Weber number. *Phys. Fluids* **22** (4), 047101.

Rayleigh, Lord 1892 On the instability of a cylinder of viscous liquid under capillary force. *Phil. Mag.* **34** (207), 145–154.

Roisman, I.V. 2009 Inertia dominated drop collisions. II. An analytical solution of the Navier–Stokes equations for a spreading viscous film. *Phys. Fluids* **21**, 052104.

Roisman, I.V., Berberović, E. & Tropea, C. 2009 Inertia dominated drop collisions. I. On the universal flow in the lamella. *Phys. Fluids* **21**, 052103.

Saroka, M.D. & Ashgriz, N. 2015 Separation criteria for off-axis binary drop collisions. *J. Fluids* **2015**, 405696.

Stone, H.A. & Leal, L.G. 1989 Relaxation and breakup of an initially extended drop in an otherwise quiescent fluid. *J. Fluid Mech.* **198**, 399–427.

SUN, K., ZHANG, P., LAW, C.K. & WANG, T. 2015 Collision dynamics and internal mixing of droplets of non-Newtonian liquids. *Phys. Rev. Appl.* **4**, 054013.

VISSER, C.W., KAMPERMAN, T., KARBAAT, L.P., LOHSE, D. & KARPERIEN, M. 2018 In-air microfluidics enables rapid fabrication of emulsions, suspensions, and 3d modular (bio)materials. *Sci. Adv.* **4** (1), eaao1175.

WILDEMAN, S., VISSER, C.W., SUN, C. & LOHSE, D. 2016 On the spreading of impacting drops. *J. Fluid Mech.* **805**, 636–655.